Deep submarine infiltration of altered geothermal groundwater on the south Chilean Margin (EarthArXiv PREPRINT)

Clementi, V.J.[1*], Rosenthal, Y.[1,2], Bova, S.C.[1,5], Thomas, E.K.[3], Wright, J.D.[2], Mortlock, R.A.[2], Cowling, O.C.[3], Godfrey, L.V.[2], Childress, L.B.[4], and Expedition 379T Scientists[†]

[1]Department of Marine and Coastal Sciences, Rutgers University, New Brunswick, NJ, USA
(*corresponding author; clementi@marine.rutgers.edu)
[2]Department of Earth and Planetary Sciences, Rutgers University, Piscataway, NJ, USA
[3]Department of Geology, University at Buffalo, Buffalo, NY, USA
[4]International Ocean Discovery Program, Texas A&M University, College Station, TX, USA
[5]Present address: Department of Geological Sciences, San Diego State University, San Diego, CA, USA
[†]A list of authors and affiliations appears at the end of the paper

Deep submarine infiltration of altered geothermal groundwater on the south Chilean Margin

Authors: Clementi, V.J.[1*], Rosenthal, Y.[1,2], Bova, S.C.[1,5], Thomas, E.K.[3], Wright, J.D.[2], Mortlock, R.A.[2], Cowling, O.C.[3], Godfrey, L.V.[2], Childress, L.B.[4], and Expedition 379T Scientists[†]

Affiliations

[1]Department of Marine and Coastal Sciences, Rutgers University, New Brunswick, NJ, USA (*corresponding author; clementi@marine.rutgers.edu)

[2]Department of Earth and Planetary Sciences, Rutgers University, Piscataway, NJ, USA

[3]Department of Geology, University at Buffalo, Buffalo, NY, USA

[4]International Ocean Discovery Program, Texas A&M University, College Station, TX, USA

[5]Present address: Department of Geological Sciences, San Diego State University, San Diego, CA, USA

[†]A list of authors and affiliations appears at the end of the paper

Abstract

Submarine groundwater discharge is increasingly recognized as an important component of the oceanic geochemical budget, but knowledge of the distribution of this phenomenon is limited. To date, reports of meteoric inputs to marine sediments are typically limited to shallow shelf and coastal environments, whereas contributions of freshwater along deeper sections of tectonically active margins like the Chilean Margin have generally been attributed to silicate diagenesis, mineral dehydration, or methane hydrate dissociation. Here we report that substantial pore water freshening on the south Chilean Margin reflects deep and focused contributions of meteorically modified geothermal groundwater, which has infiltrated marine sediments through regional fault systems. Geochemical fingerprinting of pore water data from Site J1003, recovered during D/V *JOIDES Resolution* Expedition 379T, highlights mixing between this fresh groundwater endmember and seawater, and provides the first constraints on the depth of geothermal groundwater reservoirs in the Aysén region of Patagonia. Collectively, our results identify an unappreciated locus of deep submarine groundwater and geothermal discharge along active margins, with potential implications for coastal biogeochemical processes and tectonic instability.

Introduction

A full account of the sources and sinks of solutes in the ocean is needed to constrain past and present biogeochemical cycles in the ocean. In recent decades, submarine groundwater discharge (SGD) has been shown to account for ≥5-50 percent of riverine input for several important oceanic constituents[1-3]. However, geochemical observations of SGD (≥200 mM reductions in pore water Cl^- concentration) have largely been limited to shallow shelf settings on passive margins, with scarce evidence for SGD along deeper sections of continental slopes, on active margins, or in some of the most hydrologically dynamic regions on Earth[4,5]. These data gaps intersect in Chile where despite model indications of high discharge rates (≥1000 m^2 yr^{-1})[6,7], particularly in the southern sector of the country between 40-55°S, no observational evidence for SGD exists.

Chilean groundwaters range from glacially- or meteorically-recharged aquifers[8] to geothermal aquifers[9]. Rainfall exceeding 7,500 mm yr^{-1} in southern Chile[10] promotes substantial recharge to kilometers depth through faulting in the bedrock. As a result, geothermal groundwaters in southern Chile can contain up to 50 percent meteoric fluid[11] and attain a chemical overprint, with dilute elemental concentrations (e.g., Cl^- near zero) and $^{18}O/^{16}O$ and $^{2}H/^{1}H$ isotope ratios ($\delta^{18}O$ and δD, respectively) that fall along the regional meteoric water line (MWL)[12,13]. Widespread offshore freshening of pore waters on the Chilean Margin, as indicated by 20-200 mM reductions in Cl^- compared to seawater, have been attributed to methane hydrate dissociation or mineral dehydration[14,15]. However, these prior studies lack the isotopic constraints needed to diagnostically identify source fluids[16], particularly to test for the infiltration of meteoric fluids[17-19].

In this study, we investigate the cause of substantial pore water freshening at Site J1003 (45°28.5008'S,75° 33.5020'W, 670 meters below sea level (mbsl)), which was drilled during D/V *JOIDES Resolution* Expedition 379T[20]. Site J1003 is located 50 kilometers offshore of the Taitao Peninsula at the southern terminus of the Chilean Coastal Range (CCR) and upslope from the Chile Triple Junction (Fig. 1). The North Patagonia Ice Field is ~200 km SE of J1003, though it likely extended to the shelf break during the last glacial period[21]. The Andean and Coastal mountain ranges are separated by the Liquiñe-Ofqui fault zone (LOFZ), a 1000-kilometer north-south complex of NNE lineaments[22]. The LOFZ and similar fault systems elsewhere act as a conduit for groundwater migration[9,23]. Fjord waters landward of J1003 in the Aysén region of Patagonia have geochemical signatures indicative of partial mixing with meteoric and geothermal sources, reflecting the transport of meteorically altered geothermal groundwater through the LOFZ to surface locations[12]. Using elemental and isotopic fingerprinting in high-resolution sediment pore water samples from J1003, we reveal that the meteorically altered geothermal waters that supply thermal springs at surface locations in Patagonia have also infiltrated marine sediments on the Chilean Margin, accounting for a large degree of the observed pore water freshening.

Results and Discussion

A geothermal groundwater source of freshened pore water. Pore water Cl^- at J1003 decreases from seawater values (~550 mM) at the sediment-seawater interface to ~360 mM at the base of the recovered sediment column (Fig. 2). The reduction in Cl^- is paired with strong depletions in both $\delta^{18}O$ and δD, though their largest decreases occur below 20 meters below sea floor (mbsf). Likewise, Na^+ and K^+ mirror Cl^-, linearly decreasing by 28 and 25 percent from seawater concentrations with depth, respectively. Ca^{2+}, Mg^{2+}, and Sr^{2+} concentrations also decrease with depth, but most of the reduction occurs within the upper 40 mbsf. $^{87}Sr/^{86}Sr$ becomes slightly less radiogenic (decreases) with depth, tracking many of the other profiles. In contrast, dissolved silica (DSi) concentrations increase downcore.

The depth profiles suggest that pore water at J1003 receives contributions from a freshened endmember depleted in most solutes and isotopes. Low pore water Cl^- concentrations observed in convergent margin settings have typically been attributed to methane hydrate dissociation and mineral dehydration, though anaerobic oxidation of methane, low temperature ocean-basalt interactions, clay membrane ion filtration, and SGD could also yield Cl^- substantially lower than seawater[16]. However, downcore decreases in Cl^-, $\delta^{18}O$, δD are not consistent with methane hydrate dissociation, mineral dehydration, anaerobic oxidation of methane, or fluid interactions with basalt as the primary controls on J1003 pore water chemistry, all of which increase $\delta^{18}O$ and/or δD with depth[16,24].

Remaining processes that lower Cl^-, $\delta^{18}O$, and δD include clay membrane ion filtration and SGD. Ion filtration depletes expelled pore water in ions and heavy isotopes[25]. Although Cl^-, Na^+, K^+, Ca^{2+}, Mg^{2+}, and Sr^{2+} concentrations all decrease with depth at J1003, DSi increases. Furthermore, ion filtration fractionates hydrogen more than oxygen, yielding a slope less than the MWL[26]. In contrast, $\delta^{18}O$ and δD at J1003 fall on the MWL for Chile[27] (Fig. 3). Taken together, we rule out ion filtration, leaving deep SGD as the likely dominant source of low-Cl^- pore water at J1003.

To identify the groundwater source influencing J1003 sediments, we compared $\delta^{18}O$ and δD to Cl^- (Fig. 3). Previous studies highlight linear relationships between pore water O/H isotopes and Cl^-, which when extrapolated to the freshwater source (Cl^-=0) can constrain the isotopic composition of the groundwater endmember[17,18]. Instead, non-linearity between O/H isotopes and Cl^- is observed, suggesting secondary influences from an additional endmember that shifts downcore $\delta^{18}O$ and δD towards slightly enriched values while also contributing to marked freshening (Fig. 3).

Subsurface enrichment of $\delta^{18}O$ and δD has often been interpreted as the downward diffusion of the change in isotopic composition of seawater during the last glacial period, which also increased Cl^- by ~3 percent[28]. However, the slight enrichment of $\delta^{18}O$ and δD at J1003 occurs without an increase in Cl^- (Fig. 2). Instead, a likely candidate for the observed non-linearity is methane hydrate

dissociation, which increases $\delta^{18}O$ and δD and reduces Cl^- in pore water[29]. Lower-than-expected methane hydrate concentrations have been observed in accreted sediments downslope of J1003 owing to high heat flow from subduction at the Chile Triple Junction[30,31]. Our results now provide geochemical evidence that active methane hydrate dissociation appears to be occurring off the Taitao Peninsula.

Projected endmember values for $\delta^{18}O$ (-9.8±1.71‰) and δD (-70.6±17.5‰) fall on the MWL and are in excellent agreement with modern precipitation data from southern Chile[27] and reported values from terrestrial sites in the Aysén region of Patagonia[12] (Fig. 3c). The particularly strong agreement with geothermal groundwater and meteoric endmembers ($\delta^{18}O$: -9.17±0.87‰ and -10.5±4.95‰; δD: -65.9±7.01‰ and -78.9±44.8‰, respectively) is attributable to the meteoric overprint of geothermal groundwaters in the region and points to the deep submarine infiltration of these meteorically altered geothermal groundwaters on the Chilean Margin as the dominant source of freshening at J1003. Convergence on this endmember is substantiated by linear extrapolation of deuterium excess to Cl^- equal to zero (Supplemental Fig. 1).

The (near-)linear relationships between Cl^- and Na^+, K^+, and DSi are best explained by binary mixing between seawater and the same geothermal groundwaters that supply thermal springs in the Aysén region of Patagonia[12] (Fig. 4; Supplemental Fig. 2). These mixing models indicate a geothermal groundwater contribution of ~30 percent at the base of J1003. Pore water $^{87}Sr/^{86}Sr$ at J1003 is less radiogenic than seawater and can also be attributed to mixing with regional geothermal groundwaters, which are in isotopic equilibrium with the plutonic host rock[11]. Using geothermal groundwater endmember (0.7043) from the Villarrica region just north of J1003, which has a similar bedrock lithology as the Aysén region[32], a binary mixing model for $\delta^{18}O$ and $^{87}Sr/^{86}Sr$ yields a lower contribution of ~10 percent (Supplemental Fig. 2). Nonetheless, meteorically altered geothermal groundwater contributions of 10-30 percent are sufficient to substantially modify the chemistry of sedimentary pore waters on the Chilean Margin.

Importantly, the strong agreement between pore fluid and modern meteoric isotopic data appear to rule out the emplacement of paleo-meteoric fluids at the depths of J1003 despite a more expansive Patagonian Ice Sheet during the last glacial period[21]. This contrasts with other study sites proximal to ancient ice sheets in North America and Europe, where fossil meteoric freshwater infiltrated marine sediments at the last glacial termination[19,33].

Occurrence of dolomite. The binary mixing model fails to explain non-linear reductions in Ca^{2+}, Mg^{2+}, and Sr^{2+} (Fig. 4). Instead, these trends can be attributed to the precipitation of dolomite at depth, which was documented between 15-40 mbsf[20]. At high-sedimentation sites like J1003[20], dolomitization occurs when sulfate is depleted and there is a sufficient Ca^{2+} and Mg^{2+} supply[34]. Elevated methane concentrations in the upper sections of J1003 suggest that sulfate reduction is driven by biogenic degradation of organic matter, whereas decreasing C_1/C_2 ratios towards the

base (attributable to high ethane concentrations) highlight a potential thermogenic influence at depth (Supplemental Fig. 3). Both mechanisms consume sulfate while also generating the requisite alkalinity. Furthermore, detrital silicates (high in adsorbed Mg^{2+}) readily undergo ion exchange with NH_4^+ generated during sulfate reduction[35], which potentially liberates the Mg^{2+} needed for dolomitization.

The dolomite-rich interval at J1003 coincides with sharp decreases in Ca^{2+}, Mg^{2+}, and Sr^{2+} (Fig. 2) and increased pore water Mg^{2+}/Ca^{2+} and Sr^{2+}/Ca^{2+} ratios (Supplemental Fig. 4). Such changes are consistent with dolomitization and have been observed in dolomite-rich intervals on the nearby Peru Margin[36]. In releasing H_2O, dolomitization may also contribute to observed freshening at J1003[37].

Decreases in pore water $^{87}Sr/^{86}Sr$ are attributable to binary mixing between geothermal groundwaters and seawater (Supplemental Fig 2), but the slight decrease in $^{87}Sr/^{86}Sr$ could also (in part) reflect alteration of volcanogenic material, which was invoked to explain non-radiogenic $^{87}Sr/^{86}Sr$ at Ocean Drilling Program (ODP) Site 860, located 46 km downslope of J1003[38]. Volcanogenic material comprises 0-10 percent of the bulk sediment composition at J1003[20], but its alteration would raise pore water Cl^-, Ca^{2+}, and Sr^{2+} concentrations, none of which are reported at J1003. It is plausible that Ca^{2+} and Sr^{2+} released by ash alteration are quickly consumed during dolomitization, and that any increase in Cl^- is overwhelmed by combined freshening effects from SGD, methane hydrate dissociation, and dolomite precipitation. Nonetheless, the robust binary mixing signal between $^{87}Sr/^{86}Sr$ and $\delta^{18}O$ suggests that infiltration of altered geothermal groundwater is the more likely primary control on strontium systematics at J1003 (Supplemental Figure 2).

Constraints on the geothermal groundwater reservoir and fluid migration. The ratio of Na^+ and K^+ in thermal fluids reflects temperature-dependent ion exchange between geothermal groundwater and alkali feldspars (K^+-feldspar, Na^+-feldspar)[39], and this geothermometer has been employed to characterize geothermal groundwaters in southern Chile[12,40]. If we assume that this method is also applicable in marine sediments that are influenced by geothermal groundwater, then pore water Na^+/K^+ can be used to estimate the reservoir temperature of geothermal groundwaters influencing J1003. Pore water-derived temperatures using four different equations are in excellent agreement with estimates from the Aysén thermal springs[12] (e.g., J1003: 173.68±2.06°C; Aysén: 175±14.3°C; Supplemental Table 1), and further support a geothermal groundwater connection linking the Aysén region of Patagonia and the Chilean Margin.

With ~10-30 percent of pore water influenced by meteorically altered geothermal groundwater, we infer that freshwater delivery to J1003 must be sourced from a geothermal reservoir that is substantially deeper than the penetration depth of J1003. Applying our Na^+/K^+ temperature estimates to the geothermal gradient at J1003 (53°C km^{-1}), a reservoir depth of 2.82±0.293 kmbsf

is established (Supplemental Fig. 5). Although characterization of the geothermal reservoir in the Aysén region has not yet been conducted, this estimate agrees with those for the Tinguiririca geothermal reservoir in central Chile (2-6 kmbsl)[40-42] and now provides a benchmark for future studies to test.

Despite considerable evidence for deep submarine discharge of meteorically altered geothermal groundwater at J1003, a fundamental question remains: How is this hydrogeologic connection established? Lateral migration of geothermal groundwater through the LOFZ controls the distribution of thermal springs in the Aysén region, which are often clustered near faults where buoyant hot water reaches the surface[40,42]. We now propose that this geothermal groundwater also migrates into the marine realm on the Chilean Margin. Whether fluid migration is lateral or is directly sourced from the deep reservoir cannot yet be determined. Nonetheless, our results indicate that migration of regional geothermal groundwaters not only feed thermal springs at the surface but also simultaneously delivers freshened geothermal groundwater to offshore sediments.

The absence of similar pore water features at nearby ODP Sites 859 (2760 mbsl) and 860 (2157 mbsl)[38] provide first-order depth and spatial constraints on this mechanism and suggest that infiltration of groundwater to the Chilean Margin may be focused, potentially aided by faulting within the accretionary prism[43]. This constitutes one of the deeper examples of SGD globally, but is not without precedent (e.g., ODP Leg 122 Site 760, 1970 mbsl, NW Australia[44]) and adds to a growing body of geochemical evidence for the SGD along active and passive margins[17-19,33]. Locally, our depth estimates for the Aysén geothermal reservoir may be of particular interest for efforts to harness geothermal energy for societal consumption. Globally, freshening in over pressurized accreted sediments on active margins can influence the mechanics of shallow-slip tectonism and potentially contribute to mega-thrust earthquakes that are commonly experienced in Chile and elsewhere[45]. Indeed, similar links between meteoric freshening and tectonism may operate on the Cascadia, Nankai, and Okhotsk margins, where meteorically altered geothermal groundwaters[46,47] and pore water trends similar to J1003[48,49] have been reported.

Materials and Methods

Sample collection. Pore water samples were taken from whole round samples that were immediately collected from the bottom 5-10 cm of each core section upon recovery to the catwalk, yielding a sampling resolution of ~1.5 m. In addition, one mudline sample was collected from Holes A and B in J1003. Retrieved whole rounds were capped and transferred to the shipboard geochemistry laboratory for immediate processing. In total, 40 samples were taken from J1003, with 18 samples analyzed onboard. The remainder of the pore water samples were split (~4-10 mL each), sealed in airtight glass vacuoles, and archived for shore-based analysis.

For samples that underwent shipboard analysis, the following measures were taken. First, the sediment surface of each whole round was carefully scraped to mitigate possible contamination.

Next, the whole round sample was placed in a titanium hydraulic press and subjected to 35,000 lb force for interstitial water extraction. Upon extraction, pore water was filtered through a Whatman No. 1 filter (11 μm) and 0.5 mL was discarded to avoid contamination. The remainder of fluid was filtered into a sterile syringe and filtered again through a 0.45 μm polysulfone filter.

Shipboard pore water elemental and ion analysis. Shipboard analysis of J1003 pore waters followed protocols outlined in Gieskes et al. (ref. 50), Murray et al. (ref. 51), and the International Ocean Discovery Program user manual for shipboard instrumentation. Major cations (Na^+, Ca^{2+}, Mg^{2+}, K^+) and anions (Cl^-, SO_4^{2-}) were measured on pore water samples (n=18) using a shipboard Metrohm 850 ion chromatographer (IC). Dissolved ammonium (NH_4^+) concentrations were determined using an Agilent Cary Series 100 UV-visible spectrophotometer fitted with an Agilent SPS3 autosampler. Alkalinity was determined immediately after squeezing by Gran titration with an autotitrator (Metrohm 794 basic Titrino) using 0.1M HCl at 25°C. Certain trace elements (Sr^{2+}, DSi) were measured using a shipboard Agilent 5110 SVDV ICP-AES (n=8). Precision (1σ) based on repeated measurements on IAPSO and internal standards were <3.5% for IC measurements, <3.4% for NH_4^+, and <2% for alkalinity. Reproducibility for ICP-AES measurements was ~1% for all reported elements. We refer the reader to the Expedition 379T Preliminary Report[20] for additional details on shipboard inorganic geochemical analysis of interstitial water samples.

Shipboard hydrocarbon gas analysis. Sediment gas composition was determined at a resolution of 1 sample per core for J1003 (n=9). A 3 cm^3 bulk sediment sample was collected from freshly exposed top end of a core section using a brass boring tool immediately after core recovery on the catwalk. The sediment plug was placed in a glass vial and sealed with an aluminum cap fitted with a PTFE/silicon septa for transfer to the shipboard geochemistry laboratory. The vial was heated to 70°C for 30 minutes to evolve hydrocarbon gases from the sediment. A 5 cm^3 volume of headspace gas was extracted from the sealed vial using a gas-tight 5 mL PTFE Luer lock glass syringe and injected into an Agilent/HP 6890 Series II Gas Chromatograph fitted with a flame ionization detector for analysis. Concentrations of methane (CH_4) and higher molecular weight hydrocarbons were determined and reported as parts per million by volume (ppmv) of the injected sample.

Shore-based pore water $\delta^{18}O$, δD, and $^{87}Sr/^{86}Sr$ analyses. Pore water $\delta^{18}O$ and δD were determined (n=23) using a Picarro L2130-*i* cavity ringdown laser spectrometer light isotope instrument in triplicates at the University at Buffalo following methods in van Geldern and Barth[52]. Samples were injected four times and each injection was corrected for memory and drift, and were then normalized to Vienna Standard Mean Ocean Water (VSMOW). The first injection was discarded for each sample and the remaining three analyses were aggregated into an average value with associated replicate uncertainty. Average replicate standard deviation (1 SD) was 0.02‰ for $\delta^{18}O$ measurements and 0.08‰ for δD measurements.

Additional pore water $\delta^{18}O$ measurements (n=26) were made at the Rutgers University Stable Isotope Laboratory using a FISONS OPTIMA Mass Spectrometer equipped with a MicroMass Mulitprep automatic sample processing system after water equilibration with CO_2 using standard methods[53,54]. All samples were run in duplicate. Reproducibility is estimated to be ±0.04‰ (1 SD) as determined by multiple (n=12) daily analyses of laboratory standards. Accuracy is estimated to be within 0.03‰ by comparison of North Atlantic Bottom Water with VSMOW. $\delta^{18}O$ determined on the Picarro show excellent agreement with a higher resolution record determined with IR-MS (Supplemental Fig. 6).

Pore water $^{87}Sr/^{86}Sr$ analysis (n=8) followed the Sr separation protocol of Horwitz et al.[55]. Sample volumes were calculated from shipboard elemental concentrations, targeting at least 1 µg Sr for each sample. Sample fluid was acidified to 2N using 7N HNO_3 prior to separation. Strontium was chromatographically separated from the pore water matrix using Eichrom 50-100 µm Sr Resin and different concentrations of HNO_3. Strontium was collected in 0.5N HNO_3 in acid cleaned 3 mL Savillex vials, dried down, and then dissolved in 2% by volume HNO_3 for analysis. Samples were analyzed in a wet plasma using a ThermoScientific Neptune Plus MC-ICP-MS at Rutgers University. Sr isotopes were corrected for fractionation using the measured $^{88}Sr/^{86}Sr$ ratio of 8.3752. NIST SRM 987, which was analyzed multiple times during sample analyses, yielded an $^{87}Sr/^{86}Sr$ ratio of 0.710274±0.000007 (2 SD, n=33).

Binary mixing model. By assuming that pore waters at J1003 are not altered by diagenetic reactions or other mixing processes, the elemental and isotopic composition of two pore fluid constituents in a two-endmember mixed fluid was linearly correlated following Kastner et al.[36]. Briefly,

$$Y_{IW} = X_{IW}\frac{Y_{GT} - Y_{SW}}{X_{GT} - X_{SW}} + \frac{Y_{SW}X_{GT} - Y_{GT}X_{SW}}{X_{GT} - X_{SW}}$$

where X and Y correspond to the elemental concentration or isotopic ratio of pore water constituents (e.g., Cl^- and Na^+, $\delta^{18}O$ and $^{87}Sr/^{86}Sr$). Subscripts refer to interstitial water (*IW*), geothermal groundwater (*GT*), and seawater (*SW*). In Fig. 4, X refers to Cl^- concentrations and X_{IW} is treated as a single step range of Cl^- from 18.5-540 mM.

The following table provides endmember values for seawater and geothermal groundwater, with the latter derived as the average of geothermal spring data from Negri et al. (ref. 12). For these, the error represents the 95% confidence interval based on the range of reported values, which are used to estimate the window of possible mixing lines shown in Fig. 4 and Supplemental Fig. 2. The geothermal groundwater $^{87}Sr/^{86}Sr$ and Sr^{2+} endmembers are from Held et al. (ref. 11). The mudline elemental and isotopic composition is assumed to represent the seawater endmember.

	Cl^-	Na^+	K^+	DSi	Ca^{2+}	Mg^{2+}	$\delta^{18}O$	δD	$^{87}Sr/^{86}Sr$
SW	544 mM	470 mM	10 mM	24 µM	10 mM	54 mM	-0.159 ‰	-1.7 ‰	0.7092
GT	18.5±12.4 mM	16±8.23 mM	0.523±0.311 mM	1420±276 µM	2.96±1.78 mM	0.23±0.229 mM	-9.17±0.87 ‰	-65.9±7.01 ‰	0.7043

Data Availability

The source data for J1003 shown in Fig. 2 is provided in the supplementary material. All correspondence and data requests should be addressed to V.J.C.

Acknowledgments

We would like to thank the captain and crew of the D/V *JOIDES Resolution* and JRSO for their tireless efforts during the inaugural JR100 expedition. V.J.C. would also like to thank R. Sherrell, L. Herbert, and S. Ko for fruitful discussions that improved this study. O.C.C. is supported by NSF grant EAR-IF-1652274 to E.K.T. The expedition and study were funded by NSF grant OCE-1756241 to S.C.B and Y.R., a grant from the International Association of GeoChemistry to V.J.C., and a Methane Hydrates Graduate Fellowship from the National Research Council-National Energy Technology Laboratory to V.J.C.

Author Contributions

V.J.C. and Y.R. designed the experiment. V.J.C. carried out shore-based geochemical analyses (with contributions from E.K.T., J.D.W., R.A.M., O.C.C., and L.V.G.), prepared figures, and wrote the initial manuscript. S.C.B., Y.R., and L.B.C. organized and managed the expedition. The Expedition 379T science party contributed to the collection and generation of shipboard data. All named authors contributed to the interpretation of data and revisions of this manuscript.

[†]**Expedition 379T Scientists (those not listed above):** Ivano W. Aiello[1], Alejandro Avila[2], William Biggs[3], Christopher D. Charles[4], Anson H. Cheung[5], Kimberly deLong[6], Isabel A. Dove[7], Xiaojing Du[5,8], Emily R. Estes[9], Ursula Fuentes[10], Cristina García-Lasanta[11], Steven L. Goldstein[12], Anna Golub[13], Julia Rieke Hagemann[14], Robert G. Hatfield[15], Laura L. Haynes[16], Anya V. Hess[17], Nil Irvali[18], Yael Kiro[19], Minda M. Monteagudo[20], Jonathan E. Lambert[12], Chen Li[21], William M. Longo[21,22], Sarah McGrath[5], Hailey Riechelson[3], Rebecca S. Robinson[7], John Sarao[23], Adam D. Sproson[24], Shawn Taylor[25], Yusuke Yokoyama[26], and Siyao M. Yu[17].

[1]Moss Landing Marine Laboratories, Moss Landing, California, USA. [2]Center for Oceanographic Research in the Eastern South Pacific (FONDAP-COPAS), University of Concepción, Concepción, Chile. [3]Department of Marine and Coastal Sciences, Rutgers University, New Brunswick, New Jersey, USA. [4]Scripps Institution of Oceanography, University of California, San Diego, La Jolla, California, USA. [5]Department of Earth, Environmental, and Planetary Sciences, Brown University, Providence, Rhode Island, USA. [6]Ocean Sciences Department, University of California, Santa Cruz, Santa Cruz, California, USA. [7]University of Rhode Island Graduate School of Oceanography, Narragansett, Rhode Island, USA. [8]Institute at Brown for Environment and Society, Providence, Rhode Island, USA. [9]International Ocean Discovery Program, Texas A&M University, College Station, Texas, USA. [10]Hydrographic and Oceanographic Services, Chilean Navy, Valparaíso, Chile. [11]Geology Department, Western Washington University, Bellingham,

Washington, USA. [12]Lamont-Doherty Earth Observatory, Columbia University, Palisades, New York, USA. [13]Department of Geology and Environmental Geoscience, Lafayette College, Easton, Pennsylvania, USA. [14]Department of Marine Geology and Paleontology, Alfred Wegener Institute Helmholtz Center for Polar and Marine Research, Bremerhaven, Germany. [15]Department of Geological Sciences, University of Florida, Gainesville, Florida, USA. [16]Department of Earth Science and Geography, Vassar College, Poughkeepsie, New York, USA. [17]Department of Earth and Planetary Sciences, Rutgers University, New Brunswick, New Jersey, USA. [18]Department of Earth Science and Bjerknes Centre for Climate Research, University of Bergen, Bergen, Norway. [19]Department of Earth and Planetary Sciences, Weizmann Institute of Science, Rehovot, Israel. [20]School of Earth and Atmospheric Sciences, Georgia Institute of Technology, Atlanta, Georgia, USA. [21]State Key Laboratory of Marine Geology, Tongji University, Shanghai, China. [21]Department of Environmental Studies, Macalester College, Saint Paul, Minnesota, USA. [22]Division of Environmental Health Sciences, University of Minnesota, Minneapolis, Minnesota, USA. [23]College of Geosciences, Texas A&M University, College Station, Texas, USA. [24]Biogeochemistry Research Center, JAMSTEC, Yokosuka, Japan. [25]Department of Geological Sciences and Environmental Studies, Binghamton University, Binghamton, New York, USA. [26]Atmosphere and Ocean Research Institute, The University of Tokyo, Chiba, Japan.

References

1 Moore, W. S. The Effect of Submarine Groundwater Discharge on the Ocean. *Annual Review of Marine Science* **2**, 59-88, doi:10.1146/annurev-marine-120308-081019 (2010).

2 Mayfield, K. K. *et al.* Groundwater discharge impacts marine isotope budgets of Li, Mg, Ca, Sr, and Ba. *Nature Communications* **12**, 9, doi:10.1038/s41467-020-20248-3 (2021).

3 Rahman, S., Tamborski, J. J., Charette, M. A. & Cochran, J. K. Dissolved silica in the subterranean estuary and the impact of submarine groundwater discharge on the global marine silica budget. *Marine Chemistry* **208**, 29-42, doi:10.1016/j.marchem.2018.11.006 (2019).

4 Micallef, A. *et al.* Offshore Freshened Groundwater in Continental Margins. *Reviews of Geophysics* **59**, doi:10.1029/2020rg000706 (2021).

5 Post, V. E. A. *et al.* Offshore fresh groundwater reserves as a global phenomenon. *Nature* **504**, 71-78, doi:10.1038/nature12858 (2013).

6 Luijendijk, E., Gleeson, T. & Moosdorf, N. Fresh groundwater discharge insignificant for the world's oceans but important for coastal ecosystems. *Nature Communications* **11**, 12, doi:10.1038/s41467-020-15064-8 (2020).

7 Zhou, Y. Q., Sawyer, A. H., David, C. H. & Famiglietti, J. S. Fresh Submarine Groundwater Discharge to the Near-Global Coast. *Geophysical Research Letters* **46**, 5855-5863, doi:10.1029/2019gl082749 (2019).

8 Taucare, M., Daniele, L., Viguier, B., Vallejos, A. & Arancibia, G. Groundwater resources and recharge processes in the Western Andean Front of Central Chile. *Science of The Total Environment* **722**, 137824, doi:10.1016/j.scitotenv.2020.137824 (2020).

9 Daniele, L. *et al.* Exploring the shallow geothermal resources in the Chilean Southern Volcanic Zone: Insight from the Liquine thermal springs. *Journal of Geochemical Exploration* **218**, doi:10.1016/j.gexplo.2020.106611 (2020).

10 Garreaud, R., Lopez, P., Minvielle, M. & Rojas, M. Large-Scale Control on the Patagonian Climate. *Journal of Climate* **26**, 215-230, doi:10.1175/jcli-d-12-00001.1 (2013).
11 Held, S. *et al.* Geochemical characterization of the geothermal system at Villarrica volcano, Southern Chile; Part 1: Impacts of lithology on the geothermal reservoir. *Geothermics* **74**, 226-239, doi:10.1016/j.geothermics.2018.03.004 (2018).
12 Negri, A. *et al.* Decoding fjord water contribution and geochemical processes in the Aysen thermal springs (Southern Patagonia, Chile). *Journal of Geochemical Exploration* **185**, 1-13, doi:10.1016/j.gexplo.2017.10.026 (2018).
13 Wrage, J. *et al.* Geochemistry of thermal waters in the Southern Volcanic Zone, Chile - Implications for structural controls on geothermal fluid composition. *Chemical Geology* **466**, 545-561, doi:10.1016/j.chemgeo.2017.07.004 (2017).
14 Mix, A. C., Tiedemann, R., Blum, P. & Participants, a. C. Initial Reports. *Proceedings of the Ocean Drilling Program* **202**, doi:doi:10.2973/odp.proc.ir.202.2003 (2003).
15 Scholz, F., Hensen, C., Schmidt, M. & Geersen, J. Submarine weathering of silicate minerals and the extent of pore water freshening at active continental margins. *Geochimica et Cosmochimica Acta* **100**, 200-216, doi:10.1016/j.gca.2012.09.043 (2013).
16 Kastner, M., Elderfield, H. & Martin, J. B. Fluids in convergent margins – What do we know about their composition, origin, role in diagenesis and importance for oceanic chemical fluxes? *Philosophical Transactions of the Royal Society of London Series a-Mathematical Physical and Engineering Sciences* **335**, 243-259, doi:10.1098/rsta.1991.0045 (1991).
17 Gwiazda, R. *et al.* Freshwater Seepage Into Sediments of the Shelf, Shelf Edge, and Continental Slope of the Canadian Beaufort Sea. *Geochemistry Geophysics Geosystems* **19**, 3039-3055, doi:10.1029/2018gc007623 (2018).
18 Kriete, C., Suckow, A. & Harazim, B. Pleistocene meteoric pore water in dated marine sediment cores off Callao, Peru. *Estuarine Coastal and Shelf Science* **59**, 499-510, doi:10.1016/j.ecss.2003.11.001 (2004).
19 Hong, W. L. *et al.* Discharge of Meteoric Water in the Eastern Norwegian Sea since the Last Glacial Period. *Geophysical Research Letters* **46**, 8194-8204, doi:10.1029/2019gl084237 (2019).
20 Bova, S. C. *et al.* Expedition 379T Preliminary Report, Digging Deeper with the JR100: Extending high resolution paleoclimate records from the Chilean Margin to the Eemian. *Zenodo*, doi:10.5281/zenodo.5553428 (2019).
21 Hulton, N. R. J., Purves, R. S., McCulloch, R. D., Sugden, D. E. & Bentley, M. J. The Last Glacial Maximum and deglaciation in southern South America. *Quaternary Science Reviews* **21**, 233-241, doi:10.1016/s0277-3791(01)00103-2 (2002).
22 Cembrano, J., Herve, F. & Lavenu, A. The Liquine Ofqui fault zone: A long-lived intra-arc fault system in southern Chile. *Tectonophysics* **259**, 55-66, doi:10.1016/0040-1951(95)00066-6 (1996).

23 Barton, C. A., Zoback, M. D. & Moos, D. Fluid-flow along potentially active faults in crystalline rock. *Geology* **23**, 683-686, doi:10.1130/0091-7613(1995)023<0683:ffapaf>2.3.co;2 (1995).

24 Dahlmann, A. & de Lange, G. J. Fluid-sediment interactions at Eastern Mediterranean mud volcanoes: a stable isotope study from ODP Leg 160. *Earth and Planetary Science Letters* **212**, 377-391, doi:10.1016/s0012-821x(03)00227-9 (2003).

25 Hanshaw, B. B. & Coplen, T. B. Ultrafiltration by a compacted clay membrange—II. Sodium ion exclusion at various ionic strengths. *Geochimica Et Cosmochimica Acta* **37**, 2311-2327, doi:10.1016/0016-7037(73)90106-3 (1973).

26 Coplen, T. B. & Hanshaw, B. B. Ultrafiltration by a compacted clay membrange—I. Oxygen and hydrogen isotopic fractionation. *Geochimica Et Cosmochimica Acta* **37**, 2295-2310, doi:10.1016/0016-7037(73)90105-1 (1973).

27 Sanchez-Murillo, R. *et al.* in *Andean Hydrology* (eds. D. A. Rivera, A. GodoyFaundez, & M. LilloSaavedra) 205-230 (Crc Press-Taylor & Francis Group, 2018).

28 Adkins, J. F., McIntyre, K. & Schrag, D. P. The salinity, temperature, and $\delta^{18}O$ of the glacial deep ocean. *Science* **298**, 1769-1773, doi:10.1126/science.1076252 (2002).

29 Ussler, W. & Paull, C. K. Effects of ion-exclusion and isotopic fractionation on pore-water geochemistry during gas hydrate formation and decomposition. *Geo-Marine Letters* **15**, 37-44, doi:10.1007/bf01204496 (1995).

30 Villar-Muñoz, L. *et al.* Gas Hydrate Estimate in an Area of Deformation and High Heat Flow at the Chile Triple Junction. *Geosciences* **9**, doi:10.3390/geosciences9010028 (2019).

31 Brown, K. M. *et al.* in *Proceedings of the Ocean Drilling Program, Scientific Results* Vol. 141 (eds S.D. Lewis, J. H. Behrmann, R. J. Musgrave, & S.C. Cande) 363-372 (1995).

32 Pankhurst, R. J., Weaver, S. D., Herve, F. & Larrondo, P. Mesozoic-Cenozoic evolution of the North Patagonian Batholith in Aysen, southern Chile. *Journal of the Geological Society* **156**, 673-694, doi:10.1144/gsjgs.156.4.0673 (1999).

33 van Geldern, R. *et al.* Stable isotope geochemistry of pore waters and marine sediments from the New Jersey shelf: Methane formation and fluid origin. *Geosphere* **9**, 96-112, doi:10.1130/ges00859.1 (2013).

34 Baker, P. A. & Kastner, M. Constraints on the formation of sedimentary dolomite. *Science* **213**, 214-216, doi:10.1126/science.213.4504.214 (1981).

35 Moore, G. W. & Gieskes, J. M. Interaction between sediment and interstitial water near the Japan Trench, Leg 57, Deep Sea Drilling Project. *Init. Reps. DSDP* **56-57**, 1269-1276, doi:10.2973/dsdp.proc.5657.158.1980 (1980).

36 Kastner, M. *et al.* Diagenesis and interstitial water chemistry at the Peruvian continental margin: Major constituents and strontium isotopes. *Proceedings of the Ocean Drilling Program* **112**, 413-440 (1990).

37 Morrow, D. W. Diagenesis 1. Dolomite – Part 1. The chemistry of dolomitization and dolomite precipitation. *Geoscience Canada* **9**, 5-13 (1982).

38 Zheng, Y., Froelich, P. N., Torres, M. E. & Dia, A. N. in *Proceedings of the Ocean Drilling Program, Scientific Results* Vol. 141 (eds S.D. Lewis, J. H. Behrmann, R. J. Musgrave, & S.C. Cande) (1995).
39 Giggenbach, W. F. Geothermal solute equilibria. Derivation of Na-K-Mg-Ca geoindicators. *Geochimica et Cosmochimica Acta* **52**, 2749-2765, doi:10.1016/0016-7037(88)90143-3 (1988).
40 Benavente, O. *et al.* Chemical and isotopic features of cold and thermal fluids discharged in the Southern Volcanic Zone between 32.5°S and 36°S: Insights into the physical and chemical processes controlling fluid geochemistry in geothermal systems of Central Chile. *Chemical Geology* **420**, 97-113, doi:10.1016/j.chemgeo.2015.11.010 (2016).
41 Pavez, C. *et al.* Characterization of the hydrothermal system of the Tinguiririca Volcanic Complex, Central Chile, using structural geology and passive seismic tomography. *Journal of Volcanology and Geothermal Research* **310**, 107-117, doi:10.1016/j.jvolgeores.2015.11.018 (2016).
42 Pearce, R. K. *et al.* Reactivation of Fault Systems by Compartmentalized Hydrothermal Fluids in the Southern Andes Revealed by Magnetotelluric and Seismic Data. *Tectonics* **39**, e2019TC005997 (2020).
43 Moore, J. C. & Vrolijk, P. Fluids in accretionary prisms. *Reviews of Geophysics* **30**, 113-135, doi:10.1029/92rg00201 (1992).
44 De Carlo, E. H. in *Proceedings of the Ocean Drilling Program* Vol. 122 (eds U. von Rad, B.U. Haq, & S. O'Connell) 295-308 (1992).
45 Aretusini, S., Meneghini, F., Spagnuolo, E., Harbord, C. W. & Di Toro, G. Fluid pressurisation and earthquake propagation in the Hikurangi subduction zone. *Nature Communications* **12**, doi:10.1038/s41467-021-22805-w (2021).
46 Golla, J. K. & Tepper, J. H. Comparison and controls of thermal spring chemistry in Cascade Range and Olympic Mountains geothermal provinces, Washington. *Geothermal Resources Council Transactions* **41**, 1438-1454 (2017).
47 Bragin, I. V., Zippa, E. V., Chelnokov, G. A. & Kharitonova, N. A. Estimation of the Deep Geothermal Reservoir Temperature of the Thermal Waters of the Active Continental Margin (Okhotsk Sea Coast, Far East of Asia). *Water* **13**, doi:10.3390/w13091140 (2021).
48 Tomaru, H., Torres, M. E., Matsumoto, R. & Borowski, W. S. Effect of massive gas hydrate formation on the water isotopic fractionation of the gas hydrate system at Hydrate Ridge, Cascadia margin, offshore Oregon. *Geochemistry, Geophysics, Geosystems* **7**, Q10001, doi:10.1029/2005gc001207 (2006).
49 Toki, T., Tsunogai, U., Gamo, T., Kuramoto, S. & Ashi, J. Detection of low-chloride fluids beneath a cold seep field on the Nankai accretionary wedge off Kumano, south of Japan. *Earth and Planetary Science Letters* **228**, 37-47, doi:10.1016/j.epsl.2004.09.007 (2004).
50 Gieskes, J., Gamo, T. & Brumsack, H. J. Chemical methods for interstitial water analysis aboard JOIDES Resolution. *ODP Technical Note* **15** (1991).

51 Murray, R. W., Miller, D. J. & Kryc, K. A. Analysis of major and trace elements in rocks, sediments, and interstitial waters by inductively coupled plasma-atomic emission spectrometry (ICP-AES). *ODP Technical Note* **29** (2000).

52 van Geldern, R. & Barth, J. A. C. Optimization of instrument setup and post-run corrections for oxygen and hydrogen stable isotope measurements of water by isotope ratio infrared spectroscopy (IRIS). *Limnology and Oceanography-Methods* **10**, 1024-1036, doi:10.4319/lom.2012.10.1024 (2012).

53 Epstein, S. & Mayeda, T. Variation of ^{18}O content of waters from natural sources. *Geochimica et Cosmochimica Acta* **4**, 213-224, doi:10.1016/0016-7037(53)90051-9 (1953).

54 Fairbanks, R. G. The origin of continental shelf and slope water in the New York Bight and Gulf of Mexico: evidence from $H_2{}^{18}O/H_2{}^{16}O$ ratio measurements. *Journal of Geophysical Research* **87**, 5796-5808 (1982).

55 Horwitz, E. P., Chiarizia, R. & Dietz, M. L. A novel strontium-selective extraction chromatographic resin. *Solvent Extraction and Ion Exchange* **10**, 313-336, doi:10.1080/07366299208918107 (1992).

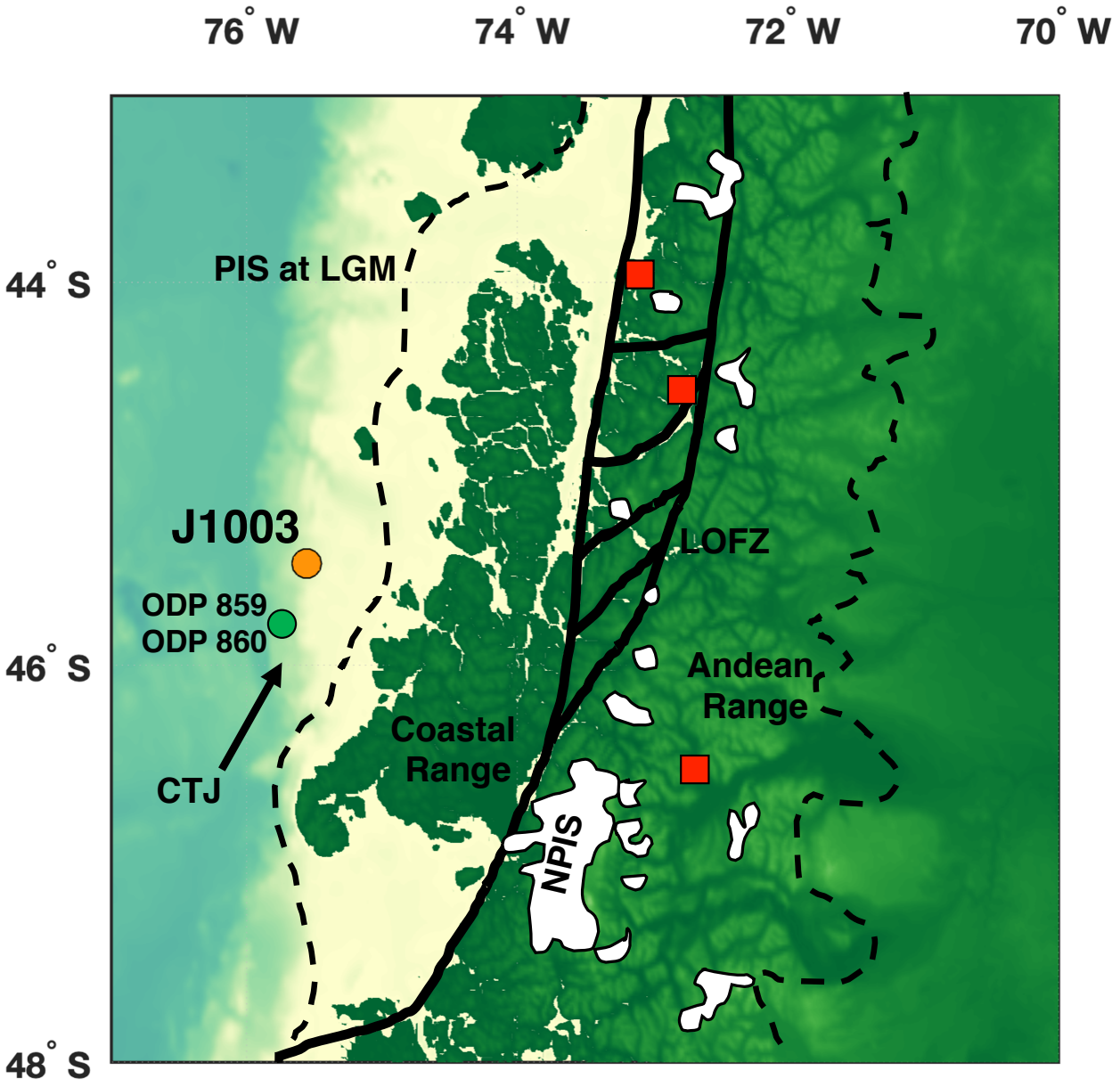

Fig. 1: Study setting. Map of the Chilean Margin showing the location of Expedition 379T Site J1003 (orange). The modern extent of the North Patagonia Ice Sheet (white patches) and during the last glacial period (dotted black line) are shown[21]. Also shown are the NNE fractures that characterize the LOFZ (thick black lines; modified after Cembrano et al. (ref. 22) and the Chile Triple Junction (CTJ). Nearby ODP Sites 859 and 860 are marked in green. The Costal Range and Andes are labeled. Red squares denote terrestrial hydrological study sites in Negri et al. (ref. 12).

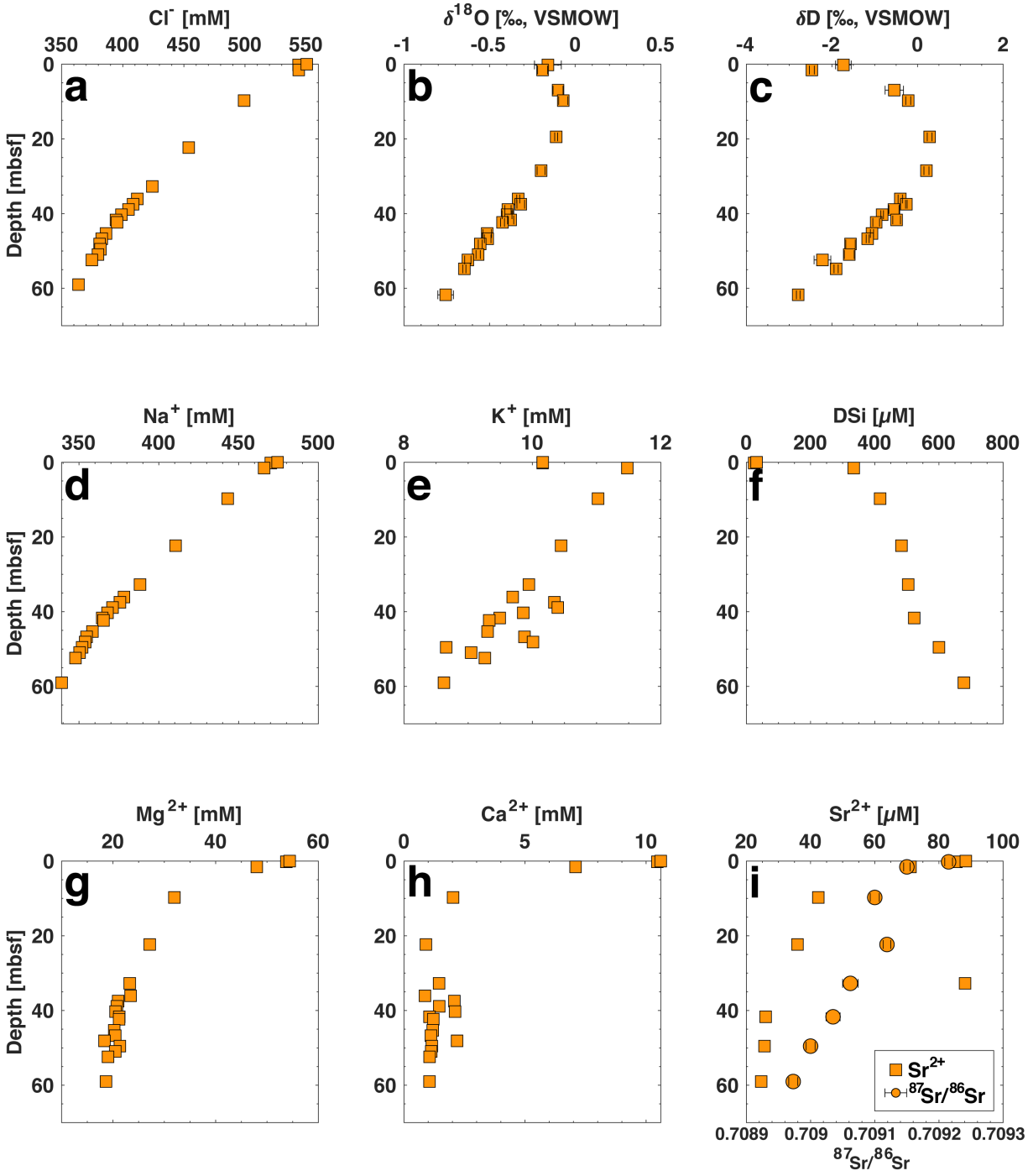

511

512 **Fig. 2: Pore water geochemical profiles for J1003**. A) Chloride (Cl^-). B) Oxygen isotope ratios
513 ($\delta^{18}O$). C) Deuterium isotope ratios (δD). D) Sodium (Na^+). E) Potassium (K^+). F) Dissolved silica
514 (DSi). G) Magnesium (Mg^{2+}). H). Calcium (Ca^{2+}). I) Strontium (Sr^{2+}) in squares, strontium isotope
515 ratios ($^{87}Sr/^{86}Sr$) in circles. Error bars in A, B, and I represent 1 standard deviation (1 SD) for each
516 sample's analysis. Depth is plotted on the vertical axis in meters below sea floor (mbsf).

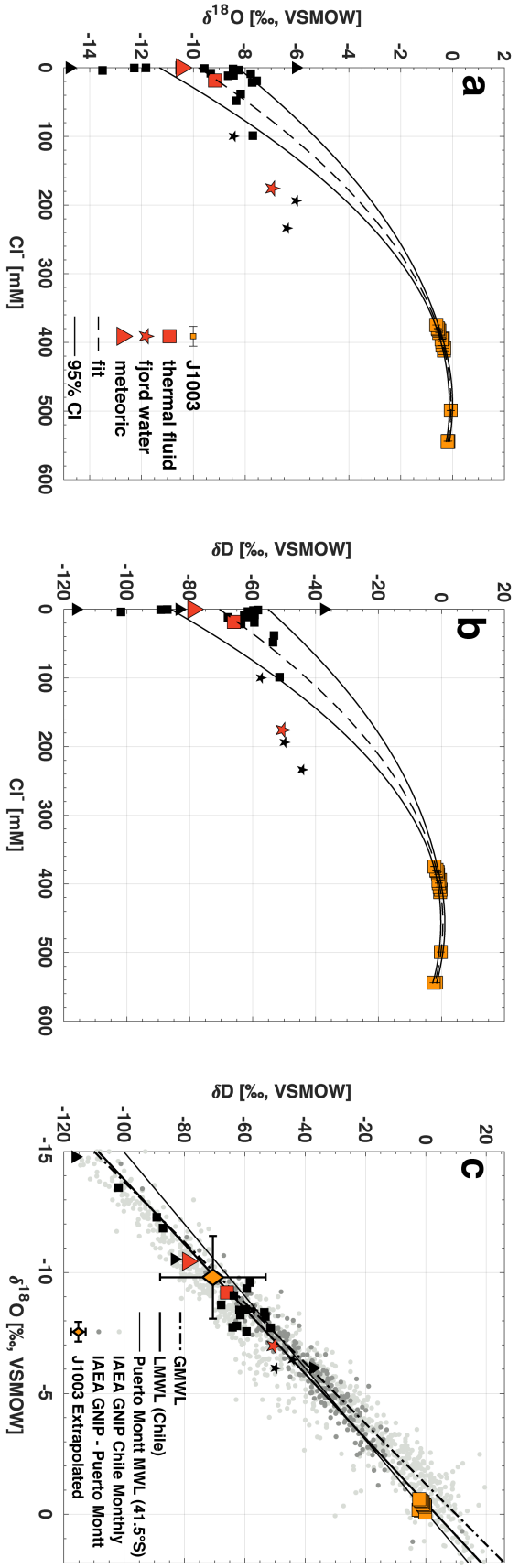
a
b
c
δ18O [‰, VSMOW]
δD [‰, VSMOW]
Cl- [mM]
J1003
thermal fluid
fjord water
meteoric
fit
95% CI
GMWL
LMWL (Chile)
Puerto Montt MWL (41.5°S)
IAEA GNIP Chile Monthly
IAEA GNIP - Puerto Montt
J1003 Extrapolated

517

Fig. 3: **Determining the groundwater origin**. A) $\delta^{18}O$ plotted against Cl^-. B) δD plotted against Cl^-. For A and B, the quadratic fit of pore water $\delta^{18}O$ and δD values, respectively, is shown by the black dotted line, with 95% confidence intervals in solid black. C) Comparison of $\delta^{18}O$ and δD with a compilation of meteoric values (grey) from Sanchez-Murillo et al. (ref. 27); data from Puerto Montt station are highlighted (dark grey). The global meteoric water line (GMWL, dotted) and those for Chile (solid), and Puerto Montt (thin) are shown. Measured and extrapolated data for J1003 are shown by the orange squares and diamond, respectively. In all plots, data for thermal fluid (square), fjord water (star), and meteoric water (triangle) from the Aysén region reported by Negri et al. (ref. 12) are shown in black, averages for each subgroup are shown in red.

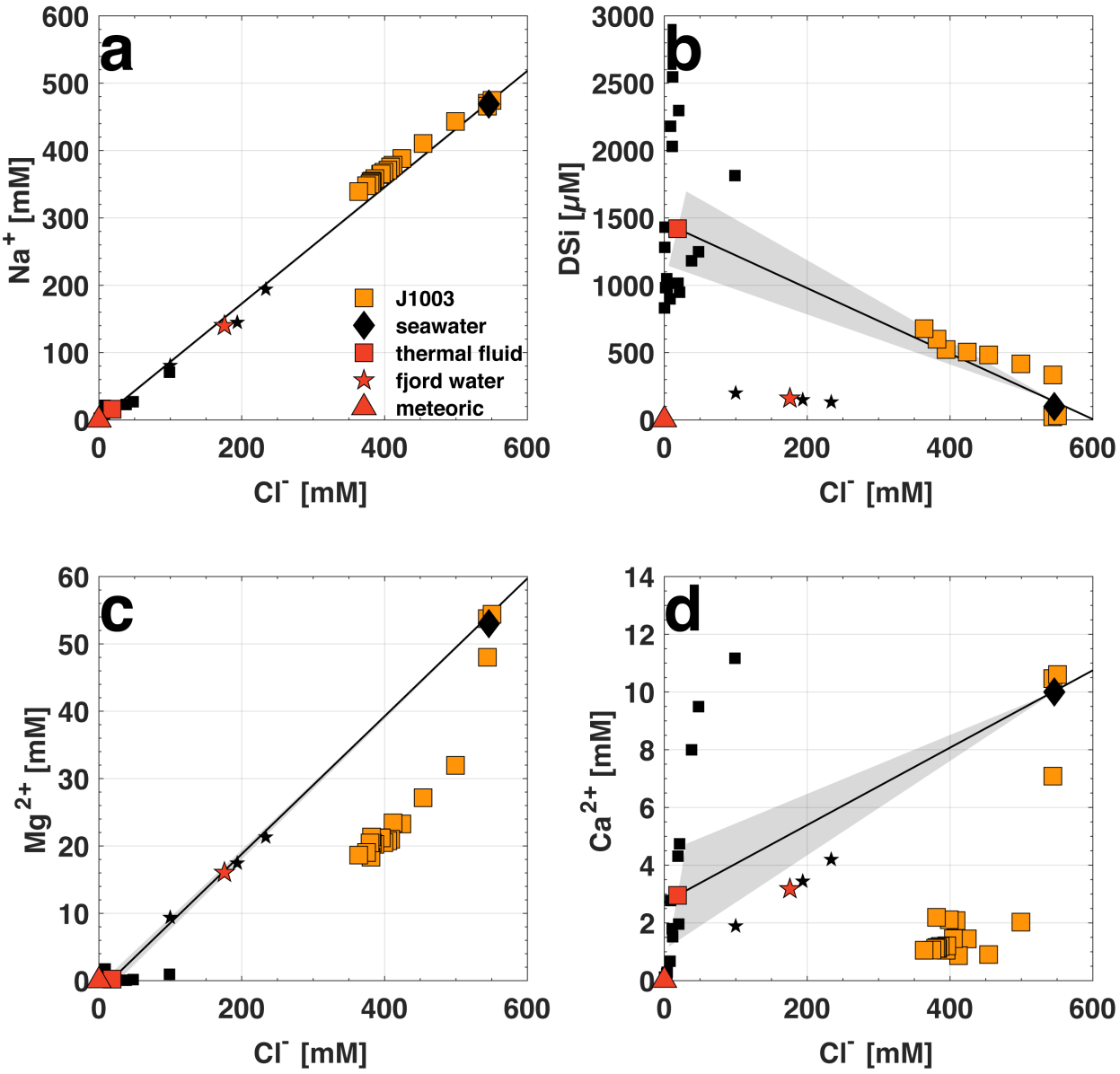

527

528 **Fig. 4: Mixing between seawater and geothermal groundwater.** A) Cl^- against Na^+. B) Cl^-
529 against DSi. C) Cl^- against Mg^{2+}. D) Cl^- against Ca^{2+}. Data for thermal fluid (square), fjord water
530 (star), and meteoric water (triangle) from the Aysén region reported by Negri et al. (ref. 12) are
531 shown in black; averages for each subgroup are shown in red. In all plots, mixing lines between
532 geothermal groundwater and seawater (black diamonds) are shown, with grey windows
533 highlighting the range of potential mixing lines derived from the minimum and maximum (95%
534 confidence interval) endmember estimates.

Supplemental Information: Deep submarine infiltration of altered geothermal groundwater on the south Chilean Margin

Contents:

1) **Supplemental Figures 1-6**
2) **Supplemental Table 1**

References

1. Supplemental Figures

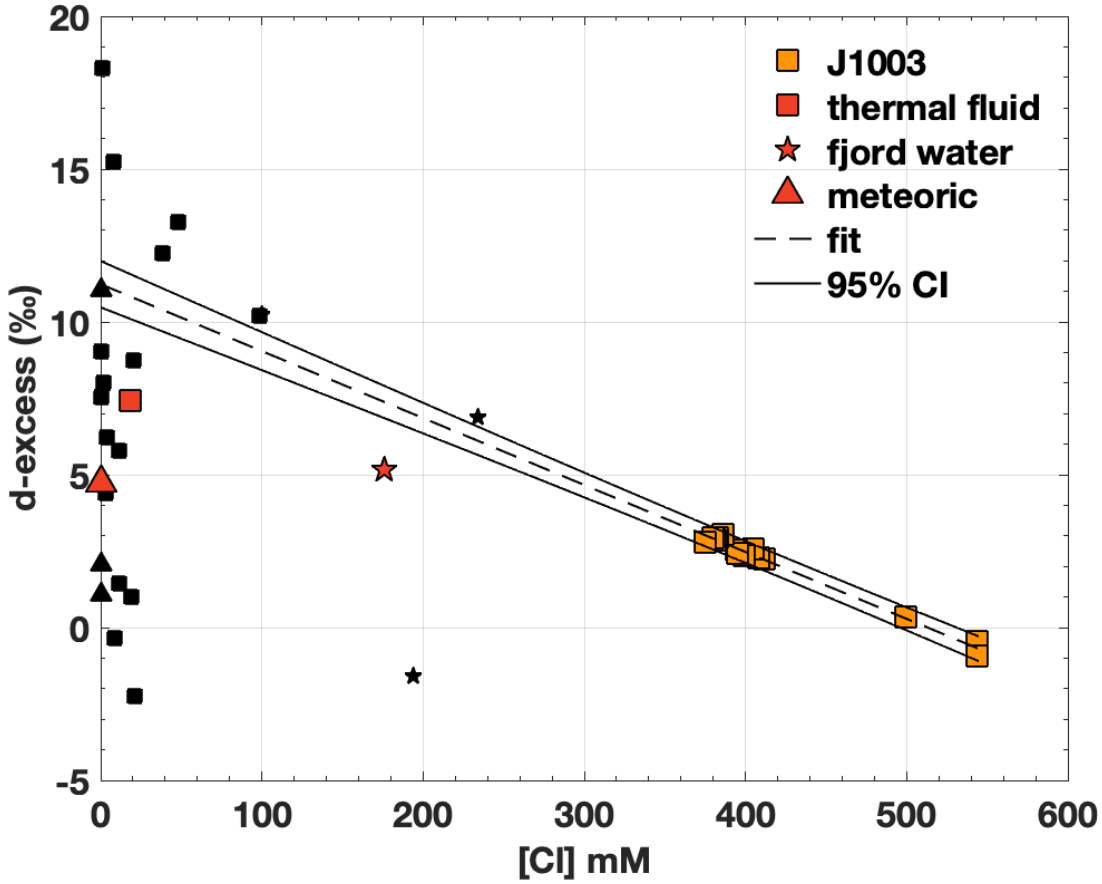

Supplemental Fig. 1. Extrapolation of deuterium excess (d-excess), which can identify source fluids[1], to Cl^- concentration equal to zero falls within the cluster of meteorically-altered geothermal groundwater values. The linear fit of Cl^- against d-excess is shown by the black dotted line, with 95% confidence intervals in solid black. Data for J1003 are shown in orange. Raw data for thermal fluid (square), fjord water (star), and meteoric water (triangle) from the Aysén region reported by Negri et al. (ref. 2) are shown in black; averages for each subgroup are shown in red.

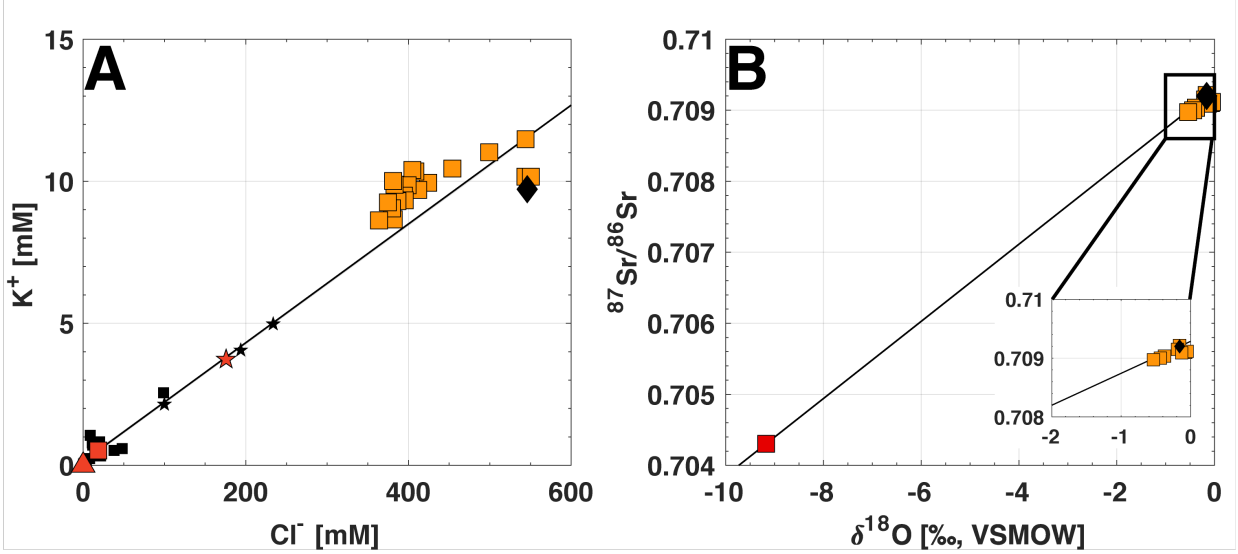

Supplemental Fig. 2. Additional mixing models. A) Cl^- against K^+ B) $\delta^{18}O$ against $^{87}Sr/^{86}Sr$. In A, data for thermal fluid (square), fjord water (star), and meteoric water (triangle) from the Aysén region reported by Negri et al. (ref. 2) are shown in black; averages for each subgroup are shown in red (see legend in Supplemental Fig. 1). In A, the mixing line is between geothermal groundwater and the first subsurface interstitial water sample (1.547 mbsf). For B, the mixing line is between geothermal groundwater and seawater. Seawater is denoted by the black diamond in both plots. The $^{87}Sr/^{86}Sr$ geothermal endmember is from Held et al. (ref. 3).

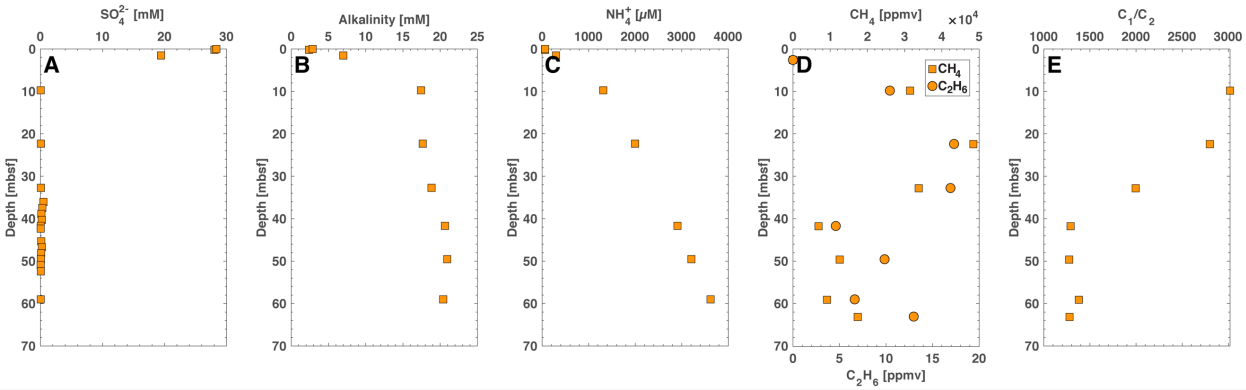

Supplemental Fig. 3. J1003 pore water profiles for A) sulfate (SO_4^{2-}), B) alkalinity, and C) ammonium (NH_4^+), D) headspace methane (CH_4, square) and ethane (C_2H_6, circle) concentrations, and E) downcore C_1/C_2 ratios. Depth is plotted on the vertical axis in meters below sea floor (mbsf). The source data for this figure are provided in the supplementary material.

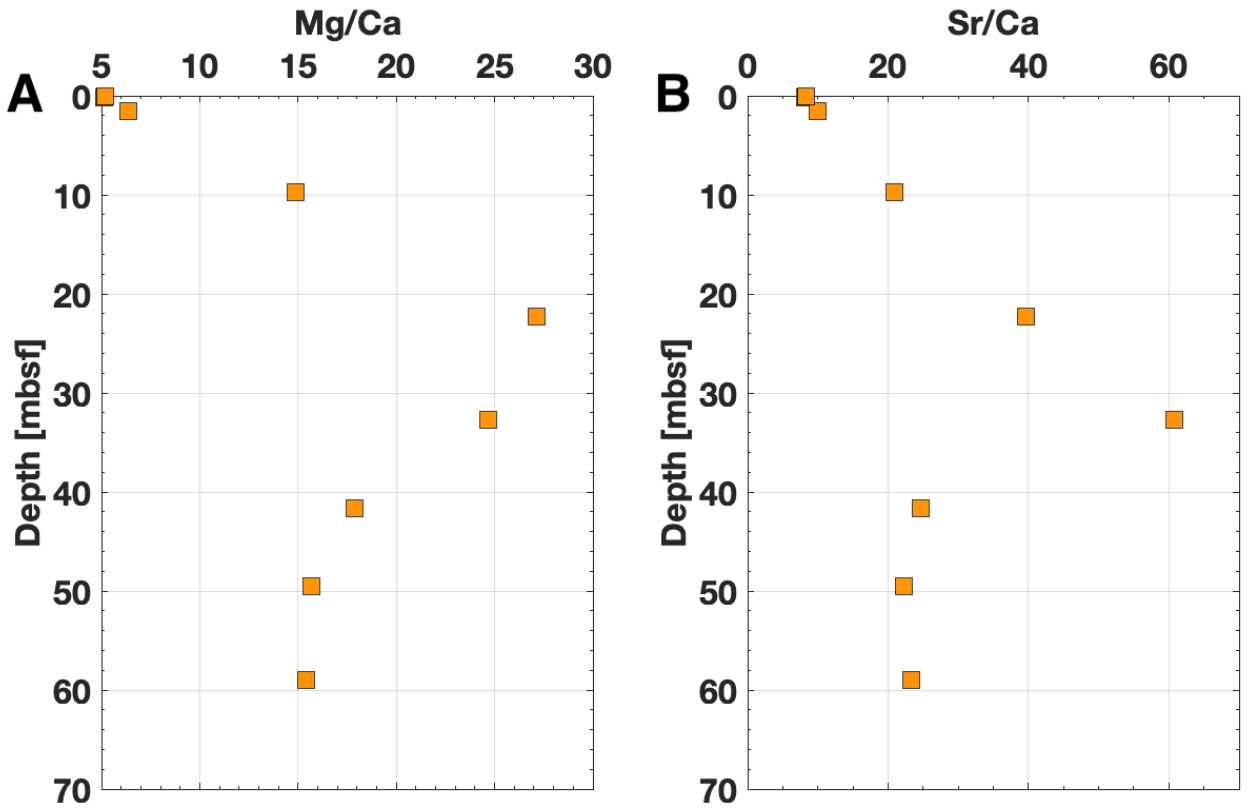

Supplemental Fig. 4. Evidence for dolomitization. Pore water ratios for A) Mg^{2+}/Ca^{2+}, and B) Sr^{2+}/Ca^{2+}. The dolomite-rich interval at J1003 occupies the sediment column between 15-40 mbsf[4], where increases in Mg^{2+}/Ca^{2+} and Sr^{2+}/Ca^{2+} are documented. Depth is plotted on the vertical axis in meters below sea floor (mbsf).

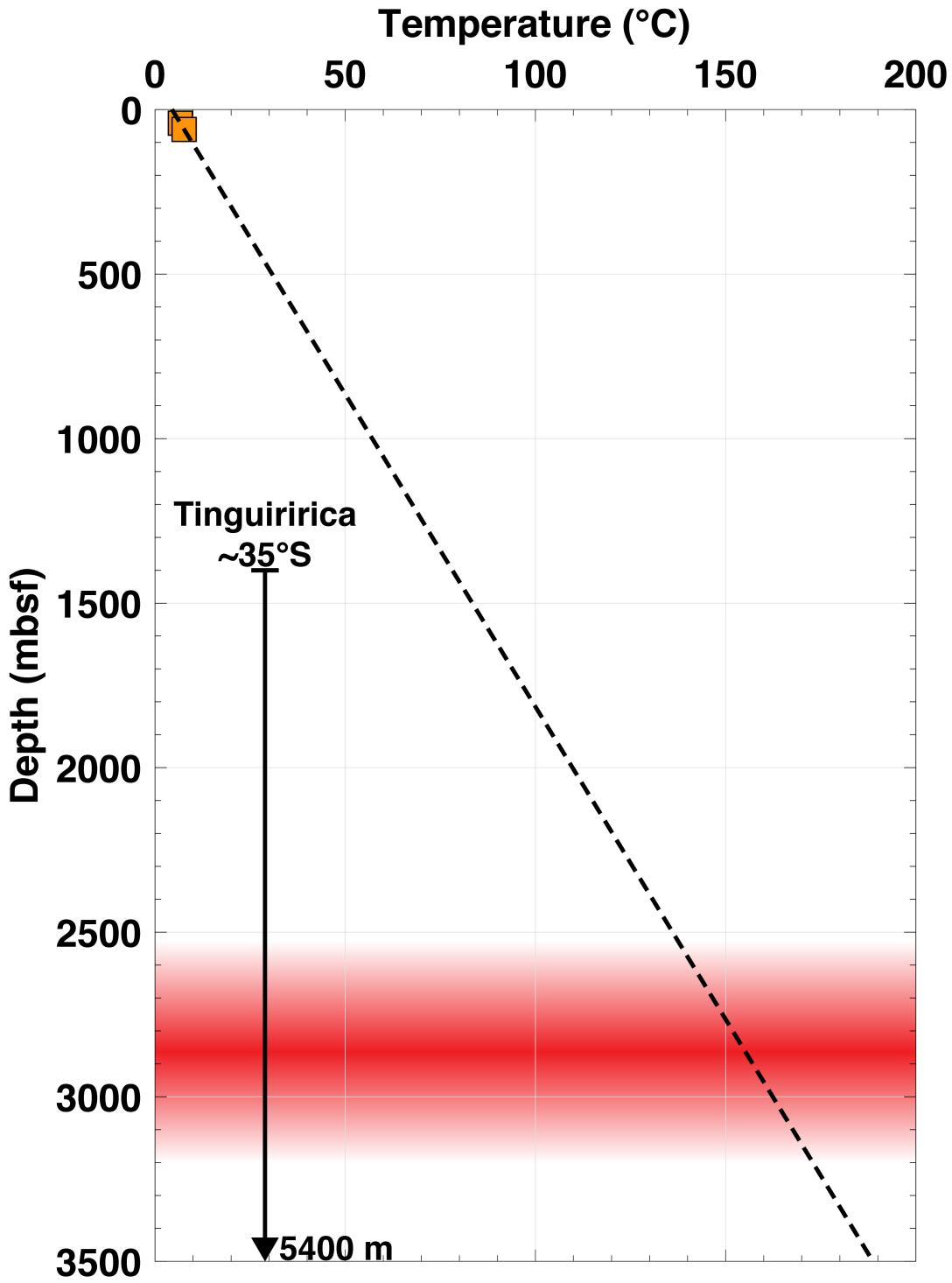

Supplemental Fig. 5. Depth estimates for the Aysén geothermal groundwater reservoir. J1003 temperature measurements from the advanced piston corer temperature tool (APCT-3) are shown in orange. The geothermal gradient for J1003 (53 °C km^{-1}) is indicated by the dotted black line. The range of Aysén geothermal groundwater temperature estimates is shown in red; the darker hue indicates average, whereas the lighter hue marks the bounds of the 95% C.I. Depth estimates from the nearby Tinguiririca geothermal reservoir (35°S) are marked by the black arrow[5,6]. Depth is plotted on the vertical axis in meters below sea floor (mbsf).

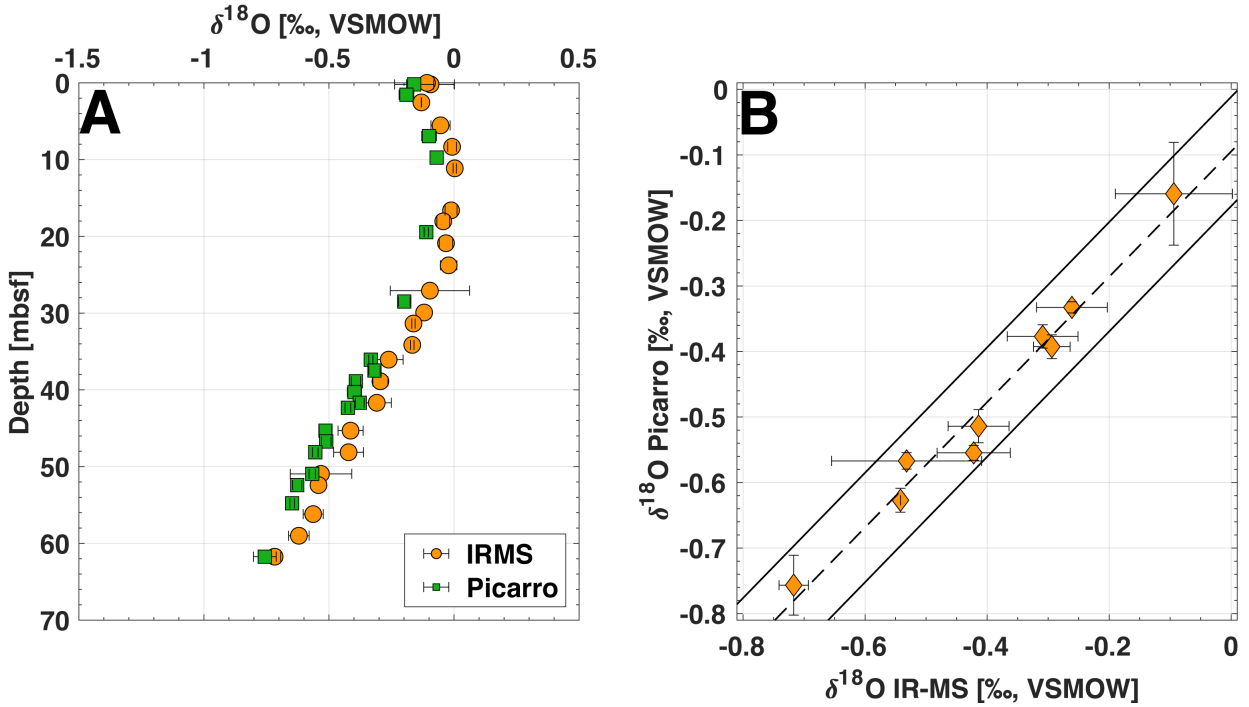

Supplemental Fig. 6. Comparing pore water $\delta^{18}O$ determination between Picarro and IR-MS methodology. A) Downcore records for IR-MS (orange) and Picarro (green) generated data. Error bars for Picarro measurements represent 1 standard deviation (1 SD) for each sample's analysis. Error bars for IR-MS measurements represent the difference between duplicate analyses for each sample. Depth is plotted on the vertical axis in meters below sea floor (mbsf). B) Cross plot comparing data from the two instruments. The dotted black line is a linear fit of the data (r^2 = 0.97, n=9) with solid lines representing upper and lower bounds of the 95% confidence interval. Data fall close to the 1:1 line, with a near constant offset (0.077±0.02‰) towards lower values determined using the Picarro.

2. Supplemental Table 1

Na^+/K^+ estimates of the Aysén geothermal groundwater reservoir temperature (GRT).				
	GRT (°C)[a]	GRT (°C)[b]	GRT (°C)[c]	GRT (°C)[d]
This Study	173.68±2.06	154.80±2.16	139.34±2.75	142.99±2.11
Negri et al.[2]	175±14.3	156±15.1	142±19.7	144.17±14.8
[a] Giggenbach [ref. 7]: T°C = 1390/(log Na/K +1.750) - 273.15 [b] Fournier [ref. 8]: T°C = 1217/(log Na/K +1.483) - 273.15 [c] Tonani [ref. 9]: T°C = 883/(log Na/K +0.780) - 273.15 [d] Nieva & Nieva [ref. 10]: T°C = 1178/(log Na/K +1.470) - 273.15 *Notes: Concentration of Na and K in mg/L. Reported error is the 95% C.I.*				

3. References

1 Pfahl, S. & Sodemann, H. What controls deuterium excess in global precipitation? *Climate of the Past* **10**, 771-781, doi:10.5194/cp-10-771-2014 (2014).

2 Negri, A. *et al.* Decoding fjord water contribution and geochemical processes in the Aysen thermal springs (Southern Patagonia, Chile). *Journal of Geochemical Exploration* **185**, 1-13, doi:10.1016/j.gexplo.2017.10.026 (2018).

3 Held, S. *et al.* Geochemical characterization of the geothermal system at Villarrica volcano, Southern Chile; Part 1: Impacts of lithology on the geothermal reservoir. *Geothermics* **74**, 226-239, doi:10.1016/j.geothermics.2018.03.004 (2018).

4 Bova, S. C. *et al.* Expedition 379T Preliminary Report, Digging Deeper with the JR100: Extending high resolution paleoclimate records from the Chilean Margin to the Eemian. *Zenodo*, doi:10.5281/zenodo.5553428 (2019).

5 Pavez, C. *et al.* Characterization of the hydrothermal system of the Tinguiririca Volcanic Complex, Central Chile, using structural geology and passive seismic tomography. *Journal of Volcanology and Geothermal Research* **310**, 107-117, doi:10.1016/j.jvolgeores.2015.11.018 (2016).

6 Benavente, O. *et al.* Chemical and isotopic features of cold and thermal fluids discharged in the Southern Volcanic Zone between 32.5°S and 36°S: Insights into the physical and chemical processes controlling fluid geochemistry in geothermal systems of Central Chile. *Chemical Geology* **420**, 97-113, doi:10.1016/j.chemgeo.2015.11.010 (2016).

7 Giggenbach, W. F. Geothermal solute equilibria. Derivation of Na-K-Mg-Ca geoindicators. *Geochimica et Cosmochimica Acta* **52**, 2749-2765, doi:10.1016/0016-7037(88)90143-3 (1988).

8 Fournier, R. O. A revised equation for the Na/K geothermometer. *Geothermal Reserouces Council Transactions* **3**, 221-224 (1979).

9 Tonani, F. B. in *Advances in European Geothermal Research*, 428-443 (Springer Netherlands, 1980).

10 Nieva, D. & Nieva, R. Developments in geothermal energy in Mexico—Part 12. A cationic geothermometer for prospecting of geothermal resources. *Heat Recovery Systems and CHP* **7**, 243-258, doi:10.1016/0890-4332(87)90138-4 (1987).